Controlling Near-Infrared Chromophore Electronic Properties through Metal−Ligand Orbital Alignment
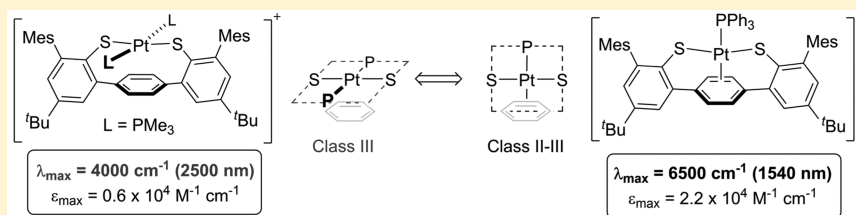
Nicole M. Mews,[†] Andreas Berkefeld,[*,†] Gerald Hörner,[*,‡] and Hartmut Schubert[†]

[†]Institut für Anorganische Chemie, Eberhard Karls Universität Tübingen, Auf der Morgenstelle 18, 72076 Tübingen, Germany
[‡]Institut für Chemie, Bioanorganische Chemie, TU Berlin, Straße des 17. Juni 135, 10623 Berlin, Germany

S *Supporting Information*

$\lambda_{max} = 4000\ cm^{-1}$ (2500 nm)
$\varepsilon_{max} = 0.6 \times 10^4\ M^{-1}\ cm^{-1}$

$\lambda_{max} = 6500\ cm^{-1}$ (1540 nm)
$\varepsilon_{max} = 2.2 \times 10^4\ M^{-1}\ cm^{-1}$

ABSTRACT: Transition-metal complexes of radical ligands can exhibit low-energy electronic transitions in the near-infrared (NIR) spectral region. NIR band energy and intensity sensitively depend on the degree of electronic coupling of the chromophore. Using the example of open-shell complexes derived from platinum and a 1,4-terphenyldithiophenol, we present a novel approach toward spectroscopically distinct NIR dyes for which the degree of electronic coupling correlates with the relative orientation of radical ligand and metal orbitals. Ligand/metal orbital alignment is modulated by auxiliary phosphine donors and selectively results in electron localized Class II−III or delocalized Class III structures that display distinct NIR transitions at 6500 and 4000 cm^{-1}.

INTRODUCTION

The systematic search for defined mixed-valent electronic structures is of high interest from a scientific and technological point of view. At the molecular level, mixed-valency can give rise to intense electronic transitions in the low-energy near-infrared (NIR) spectral range, depending on the respective degree of charge delocalization.[1] With regard to application, for instance, controlling NIR absorptivity is relevant for glass optical fiber technology to modulate signal transduction in the 1300 and 1550 nm spectral ranges. Transition energy, intensity, and spectral width of an NIR band are determined by the respective type of charge-transfer (CT) mechanism.[2] Examples include π−π* type interligand (LL) and metal-to-ligand (ML) CT in ligand radical ion complexes of bipyridine[1a,b,2a,3] or aminiumpolypyridine,[4] and metal centered interconfigurational transitions in complexes of Os^{III}.[2a] Alternatively, electronic coupling of coplanar, π-conjugated mixed-valent ligands at a planar (d^8-)metal site can give rise to intense ligand based intervalence (LLIV) CT or charge-resonance (CR) transitions, again depending on the degree of charge delocalization.[1a,5] Prominent examples of ligand systems are benzenedi-[6] and tetrathiophenols,[7] catechols[1c,8] and amino derivatives thereof,[9] dithiolenes,[10] salens[11] and thiosalens.[12]

Modification of chromophore systems has previously been achieved through variation of a number of parameters such as the conformational flexibility and substitution pattern of ligand(s), and the choice and number of metal bridges. A notable example is the family of transition-metal complexes of salen ligands schematized on the bottom left of Figure 1. In
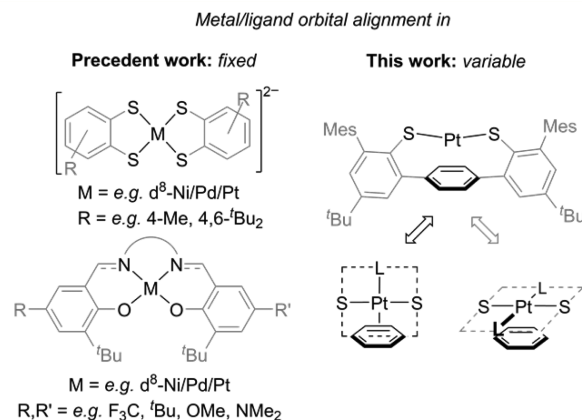

Metal/ligand orbital alignment in

Precedent work: *fixed* M = e.g. d^8-Ni/Pd/Pt R = e.g. 4-Me, 4,6-^{t}Bu$_2$

M = e.g. d^8-Ni/Pd/Pt R,R' = e.g. F$_3$C, ^{t}Bu, OMe, NMe$_2$

This work: *variable*

Figure 1. Left: Fixed alignment of the coordination plane of group 10 d^8-metal ions of 1,2-benzenedithiol and salen ligands; Right: 1,4-terphenyldithiophenolato complexes of d^8-Pt with variable alignment of metal coordination plane and ligand.

solution of a weakly coordinating solvent such as CH$_2$Cl$_2$, the one-electron oxidized complexes exist in the form of valence tautomers (thio)phenoxyl/(thio)phenolato-M^{n+} and di(thio)-phenolato-M$^{(n+1)+}$, depending on temperature.[11c,13] The d-electron configuration of the metal bridge does not determine the character of the radical ligand orbitals but their relative contribution to the highest singly occupied MO (SOMO), and

so determines the strength of electronic coupling of the (thio)phenoxyl and (thio)phenolato sites.[11d,12,14]

Transition energy and intensity of the NIR bands correlate with the strength of electronic coupling along the metal bridge. For a given metal bridge, e.g., Ni, the electronic structure of the SOMO can be varied between delocalized Class III and electron localized Class II structures by changing the electronic properties of the *para*-substituents at the phenol moiety, cf. Figure 1, from, e.g., ^tBu with $\nu_{max} = 4700$ cm^{-1} ($\varepsilon_{max} = 2.6 \times 10^4$ M^{-1} cm^{-1}, $\Delta\nu_{1/2} = 660$ cm^{-1}, Class III)[15] to NMe$_2$ with $\nu_{max} = 8500$ cm^{-1} ($\varepsilon_{max} = 0.4 \times 10^4$ M^{-1} cm^{-1}, $\Delta\nu_{1/2} = 6650$ cm^{-1}, Class II).[11d,16] Expansion of the ligand field at Ni through coordination by axial pyridine donors[11c,12,17] or solvent[13a] shifts the valence tautomer equilibrium in favor of the bis(thio)-phenolato-Ni(III) form. For a given ligand system, e.g., R, R′ = ^tBu, the strength of electronic coupling of the phenoxyl/phenolato moieties increases in the series Pd (Class II−III) < Ni (Class III) < Pt (Class III) and is associated with a blue-shift of ν_{max} and an increase of ε_{max} (10^4 M^{-1} cm^{-1}) in the same order 4100 (1.6) < 4700 (2.6) < 5450 (3.3) cm^{-1}.[15b] Neese and Wieghardt had also substantiated the correlation of increasing superexchange efficiency and a blue-shift of low-energy transitions ν_{max} for Class III 1,2-dithiosemiquinonato/dithiolato complexes $[(S_2^{2-})M^{II}(S_2^{\bullet -})]^-$, $S_2^{2-} = 4,6$-$^tBu_2$-1,2-C$_6$H$_2$S$_2$ (cf. top left of Figure 1), which follow the order M^{II} = Pd ($\nu_{max} = 8800$ cm^{-1} [$\varepsilon_{max} = 2.5 \times 10^4$/M^{-1} cm^{-1}]) < Pt (11100 [1.9×10^4]) < Ni (11200 [1.5×10^4]).[6b,c] Herein, we report on a novel approach that uses the relative orientation of radical ligand and metal bridge orbitals as the key element to control the electronic and spectroscopic properties of a metal complex NIR chromophore.

■ RESULTS AND DISCUSSION

As summarized in Figures 1 and 2, open-shell complexes of Pt of a 1,4-terphenyldithiophenol have been prepared, and whose
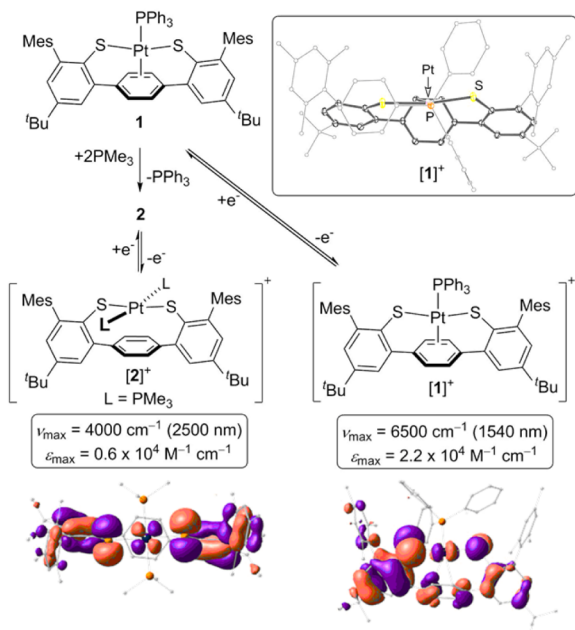

Figure 2. Preparation, structure, and key NIR absorption bands of complex cations $[2]^+$ and $[1]^+$. Bottom: Respective SOMOs (α-HOMOs) at the BLYP-35/TZVP/ZORA level; Inset: Molecular structure of $[1]^+$.

distinct NIR absorption profiles correlate with the parallel, $[1]^+$, or orthogonal, $[2]^+$, orientation of the metal coordination plane relative to the coplanar aryl-S π-systems. Auxiliary phosphine ligands aid in modulating the alignment of the metal coordination plane which determines the electronic character of the $[^{Ar}S−Pt−S^{Ar}]^{\bullet +}$ core structure and is responsible for the distinct NIR absorptivity of $[1]^+$ and $[2]^+$. Highest energy singly occupied molecular orbitals (SOMO; cf. bottom of Figure 2) are characterized by an intraligand electronic coupling via out-of-plane and in-plane metal d-orbitals in $[1]^+$ and $[2]^+$, respectively.

Parent complex **1** has been prepared by salt metathesis from *trans*-Pt(py)$_2$Cl$_2$,[18] py = pyridine, ligand dipotassium salt, and PPh$_3$ in toluene solution, and is isolable as a light green crystalline solid in 49% yield. Exchange of PPh$_3$ for two PMe$_3$ affords yellow **2** quantitatively. Single crystal structure and solution NMR data provided in the Supporting Information (Figures S13 and S14, and Table S6, SI) support the parallel and orthogonal structural alignment of the metal coordination plane and S-aryl π-systems in neutral **1** and **2**, respectively.

One-electron oxidation using the 1,1′-diacetylferrocene cation yields the intensely colored ions $[1]^+$ and $[2]^+$ quantitatively. Cation $[1]^+$ is isolable as the N(SO$_2$CF$_3$)$_2^-$, NTf$_2^-$, salt in the form of maroon microcrystals in 77% yield, and displays a constant $\mu_{eff}([1]^+) = 2.3$ in CD$_2$Cl$_2$ solution over a 213−313 K range as expected for a $S = 1/2$ system. In clear contrast, $[2]$NTf$_2$ seems to be a kinetic reaction product and is metastable at $T \leq 253$ K. Dark blue-purple solutions deteriorate noticeably if warmed to $T \geq 273$ K as the result of a redox reaction that involves thermally induced dissociation of one PMe$_3$ ligand from Pt. Variable temperature (VT) ^{1}H and ^{31}P NMR spectroscopic monitoring indicates the partial reformation of **2** along with ill-defined diamagnetic products. Notably, addition of one equivalent of PMe$_3$ or, alternatively, (H$_5$C$_5$)$_2$Co to $[2]$NTf$_2$ at $T = 203$ K instantaneously results in the almost quantitative (≥95%) reduction back to **2**, as evidenced by ^{1}H and ^{31}P NMR spectroscopy (cf. Figures S2 and S3, SI), proving the reaction stoichiometry correct. Accordingly, the susceptibility of a CD$_2$Cl$_2$ solution of an in situ prepared sample correlates with a constant $\mu_{eff}([2]^+) = 2.3$ at temperatures 193−233 K, identical to the value $\mu_{eff}([1]^+)$ obtained for the thermally robust $[1]^+$.

Chemical oxidation is consistent with the results of cyclic voltammetry at a Pt disc electrode in 0.1 M nBu$_4$NPF$_6$ CH$_2$Cl$_2$ solution at 290 K. Anodic potential sweeps relative to the $[Fc]^+$/Fc couple, Fc = ferrocene, showed oxidation events at formal potentials of 60 and 727 mV in case of **1** and 117, 618, and 719 mV for **2**. All redox events are electrochemically reversible for **1**, whereas in case of **2** the second oxidation wave at 618 mV is not; cf. Figures S4−S5 and Tables S1−S4, SI. The redox couple **2**/$[2]^+$ at 117 mV displays Nernstian behavior if the potential sweep direction is reversed at $E \leq 400$ mV but becomes *chemically* partially irreversible, $i_{p,red}/i_{p,ox} < 1$, otherwise. On the basis of this observation, the electrochemically reversible event at 719 mV is assigned to the $[2]^+$/$[2]^{2+}$ couple. Potential differences $\Delta E_{1/2}$ equal to 667 mV and 602 mV between the first and second redox couple of **1** and **2**, respectively, indicate that electronic stabilization of both monocations is sizable, and points to an extensive electronic coupling of redox-sites across Pt in both cases.

The molecular structure of $[1]^+$ shown in Figure 2 has been determined by X-ray crystallography.[19] The general structural features indicate a contraction of the ligand-sphere upon

oxidation of **1**; Pt-π-arene, Pt–S, and C–S distances decrease by 0.02, 0.05, and 0.02 Å, respectively, whereas the Pt–P bond is elongated by 0.04 Å. These geometric changes reflect the overall π^*-character of the β-LUMO of [**1**]$^+$ (see Figure 5a) that is characterized by significant Pt–S, Pt–C$_{arene}$, and S–C$_{S\text{-arene}}$ interactions. Notably, Neese and Wieghardt also reported on the reduction of Pt–S and S–C$_{arene}$ bond lengths for the one- and two-electron oxidized forms [(S$_2$$^{2-}$)-Ni^{II}(S$_2$$^{\bullet-}$)]$^-$ and [Ni^{II}(S$_2$$^{\bullet-}$)$_2$] of the parent complex [(4,6-(^{t}Bu)$_2$-1,2-C$_6$H$_2$S$_2$)$_2$Ni^{II}]$^{2-}$.[6b] In comparison to **1**, the square planar ligand environment at Pt is less distorted in [**1**]$^+$, and is indicated by an increase of the *trans*-P-Pt-(C≡C) angle by 13° to 175°.

The quality of the diffraction data allowed for a highly accurate elucidation of the bond lengths, which are within ±0.009 Å (3σ) for [**1**]$^+$ as compared to ±0.021 Å for **1**. In particular, it renders the observed anisotropy in the Pt–S bond lengths (Δd(Pt–S) = 1.4 pm) a significant feature. DFT-derived (BP86-D3/TZVP/ZORA) structural metrics of [**1**]$^+$ confirm the experimentally observed dissymmetry about the S–Pt–S moiety (Δd(Pt–S) = 3.1 pm) and also indicate a dissymmetry of the electronic structure of the [^{Ar}S–Pt–S^{Ar}] core in [**1**]$^+$. The close consistency of computed and experimental metrics, obtained in an experimentally calibrated DFT study of **1**, **2**, [**1**]$^+$ (Table S5, SI) and a related reference system [(S$_2$$^{2-}$)Pt(S$_2$$^{\bullet-}$)]$^-$, S$_2$$^{2-}$ = 4-Me-1,2-C$_6$H$_2$S$_2$, reported by Gray and co-workers[6a] validates the optimized structure of elusive [**2**]$^+$. As seen for **1** and [**1**]$^+$, the structural features of [**2**]$^+$ greatly echo those of neutral **2**, particularly with respect to mutual orientation of the aryl-S π-systems and the coordination plane at Pt. The computed Pt–S bond contraction is slightly more pronounced in case of [**2**]$^+$ as compared to [**1**]$^+$; importantly, however, the contracted S–Pt–S vector is clearly isotropic in the case of [**2**]$^+$. These qualitative differences in the geometric structures of [**1**]$^+$ and [**2**]$^+$ persist in their electronic structures, as suggested by DFT results and clearly pointed out by EPR and UV/vis/NIR spectroscopy. Analysis of spin densities ρ computed at the BLYP-35-D3/TZVP/ZORA[20] level of theory identifies both cations as being predominantly ligand-centered radicals (cf. Table S8, SI). For both ions [**1**]$^+$ and [**2**]$^+$ > 99% of one spin integrate within the [^{Ar}S–Pt–S^{Ar}] moiety but only ~11% localize at Pt. On the basis of the data, we suggest partial localization of spin on one ^{Ar}S-moiety of [^{Ar}S–Pt–S^{Ar}]$^{\bullet+}$ (ρ(^{Ar}S)/ρ(Ar$'$S$'$) ≈ 1.91) in the case of [**1**]$^+$, whereas a fully delocalized spin of a Class III [^{Ar}S–Pt–S^{Ar}]$^{\bullet+}$ system prevails for [**2**]$^+$ (ρ(^{Ar}S)/ρ(Ar$'$S$'$) ≈ 0.99).

CW X-Band EPR spectral properties of isolated [**1**]NTf$_2$ and in situ generated [**2**]NTf$_2$ in an 1:1 CH$_2$Cl$_2$/toluene solvent mixture corroborate the theoretical analysis and further substantiate the qualitative differences in their electronic structures as indicated by diverging sizes of g-anisotropy (Δg) and hyperfine coupling (*hfc*). In particular, while stronger g-anisotropy prevails for [**1**]$^+$, cation [**2**]$^+$ displays stronger overall *hfc* to naturally abundant ^{195}Pt (I = 1/2, 34%). Pertinent data are collected in Table 1. Although no further couplings are resolved in the rhombic derivative spectra, the decrease of line-widths observed for [**1**]$^+$ along $\Delta\nu_{1/2,1}$ = 76 > $\Delta\nu_{1/2,2}$ = 43 > $\Delta\nu_{1/2,3}$ = 13 MHz with increasing magnetic field suggests a weak contribution of ^{31}P-*hfc*. Both cations reveal moderate anisotropies in their g-values, reflecting the involvement of metal orbitals in the SOMO. This is corroborated by the clear distinction in g-anisotropies between [**2**]$^+$ (Δg = 0.078) and semiquinonate complexes of Pt^{II} (Δg = 0.022) reported by

Table 1. X-Band EPR Spectral Data of [1]$^+$ and [2]$^{+a,b}$

	g_1	g_2	g_3	Δg	A_1	A_2	A_3
[**1**]$^+$	2.174	2.082	2.005	0.169	175	184	239
[**2**]$^+$	2.124	2.063	2.046	0.078	325	490	291

^{a}NTf$_2$-salts, CH$_2$Cl$_2$/C$_7$H$_8$ glass, 77 K; A(^{195}Pt(I = 1/2, 34%)) in MHz. ^{b}[**1**]$^+$, 293 K: g_{iso} = 2.089, A_{iso}(^{195}Pt) = 191.

Halcrow,[21] in which the radical is essentially ligand-localized. On the other hand, significant g-anisotropies reported for mixed-valent complexes [(S$_2$$^{2-}$)Pt(S$_2$$^{\bullet-}$)]$^-$ (S$_2$$^{2-}$ = 4-Me-1,2-benzenedithiolato, Δg = 0.419, by Gray;[6a] S$_2$$^{2-}$ = 3,5-^{t}Bu$_2$-1,2-benzenedithiolato, Δg = 0.38 (21% calculated spin density at Pt) by Neese and Wieghardt[6b]) were correlated to an increase of Pt-character in the SOMO according to computational data. Similarly, observed $\Delta\Delta g$([**1**]$^+$–[**2**]$^+$) = 0.092 and overall larger A(^{195}Pt) for [**2**]$^+$ may be attributed to different relative contributions of ligand and metal orbitals to the SOMOs. However, computed spin-densities amount to ~11% at Pt for both compounds and contradict this picture, indicating that additional factors are active here. For instance, mixing of a metal-centered excited state to the ground state of [**1**]$^+$ by spin–orbit coupling may be significant. Note that combining dipolar and orbital terms may compensate the contribution of the Fermi contact term to A(^{195}Pt).[6b]

The difference of the electronic structures of the [^{Ar}S–Pt–S^{Ar}]$^{\bullet+}$ cores between [**1**]$^+$ and [**2**]$^+$ is substantiated by the observation of distinctly different NIR absorption bands. The neutral complexes are optically transparent in the NIR spectral region, with the lowest-energy transitions λ_{max} (ε_{max}/M^{-1} cm^{-1}) being observed at 578 nm (200, in 1,2-C$_6$F$_2$H$_4$) for **1** and 318 nm (1.4 × 10^4, in CH$_2$Cl$_2$) for **2**. Upon oxidation of **1** and **2**, intense absorption bands develop across the visible range and in the NIR region. Table 2 summarizes the position, intensity,

Table 2. Band Shape Parameters and Solvent Dependence for Low-Energy NIR Transitions of [1]$^+$ and [2]$^{+a,b}$

	solvent	ε_{solv}^{c}	ν_{max} (cm^{-1})	ε_{max} (M^{-1} cm^{-1})	$\Delta\nu_{1/2}$ (cm^{-1})
[**1**]$^+$	C$_7$H$_8$	2.39	6570	15000	1570
[**1**]$^+$	CH$_2$Cl$_2$	8.93	6470	22000	1470
[**1**]$^+$	1,2-C$_6$F$_2$H$_4$	13.4	6500	17000	1510
[**1**]$^+$	C$_4$H$_6$O$_3$	66	6580	16000	1680
[**2**]$^+$	C$_7$D$_8$	~2.4^c	4050	4000	2000
[**2**]$^+$	CH$_2$Cl$_2$	8.93	4000	6000	1700

^{a}NTf$_2$-salts; [**2**]NTf$_2$ generated in situ at 213 K. ^{b}Measurement T = 296 K for [**1**]NTf$_2$ and 203 K for [**2**]NTf$_2$. ^{c}Solvent dielectric constants taken from literature,[22] estimate for ε_{solv}(C$_7$D$_8$) ≈ ε_{solv}(C$_7$H$_8$).

line-width at half height, and solvent dependence of ν_{max} for the NIR bands of [**1**]NTf$_2$ and [**2**]NTf$_2$. Compound [**1**]NTf$_2$ features an intense, narrow, slightly asymmetric transition at 6500 cm^{-1} (1540 nm, ε_{max} = 1.7 × 10^4 M^{-1} cm^{-1}, $\Delta\nu_{1/2}$ = 1550 cm^{-1}) in 1,2-C$_6$F$_2$H$_4$ solution. As depicted in Figure 3, the dependence of ν_{max}, ε_{max}, and $\Delta\nu_{1/2}$ on solvent relative permittivity is small for a range of solvents that spans in polarity from toluene to propylene carbonate ($\Delta\varepsilon_{solv}$ ~ 63, cf. Table 2). There is no clear correlation of the transition intensity with solvent polarity. The largest intensity is recorded in moderately polar CH$_2$Cl$_2$, whereas the data in toluene, 1,2-C$_6$F$_2$H$_4$ and propylene carbonate are close to identical, despite their distinct permittivities (cf. Table 2; similar observations

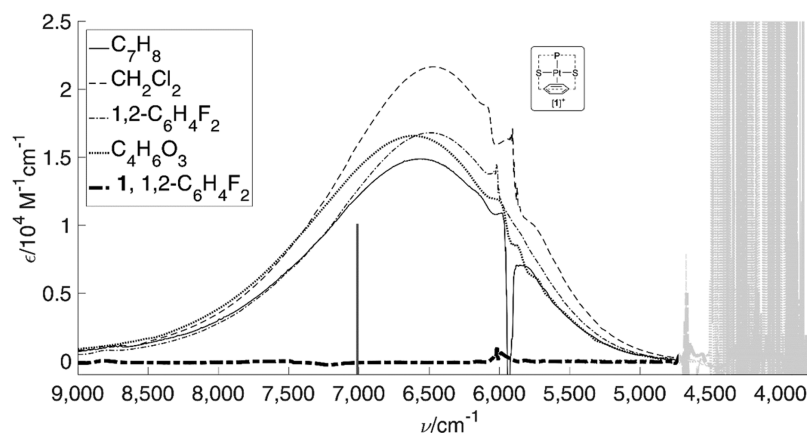**Figure 3.** NIR absorption profiles of [1]NTf$_2$ in solvents of different relative permittivity[22] (ε_{solv}) taken at T = 296 K: C$_7$H$_8$ (2.39), CH$_2$Cl$_2$ (8.93), 1,2-C$_6$F$_2$H$_4$ (13.4), and C$_4$H$_6$O$_3$ (66) (cf. Figure S9 for spectra in 40000−4500 cm^{-1} range); Spectra of **1** were taken in 1,2-C$_6$F$_2$H$_4$. Solid gray bar: TD-DFT derived ν_{max}(TD-DFT) = 7007 cm^{-1} (f_{osc}(TD-DFT) = 0.20). Strong solvent background absorption at ν_{max} < 4500 cm^{-1} attenuated (light gray) for clarity.
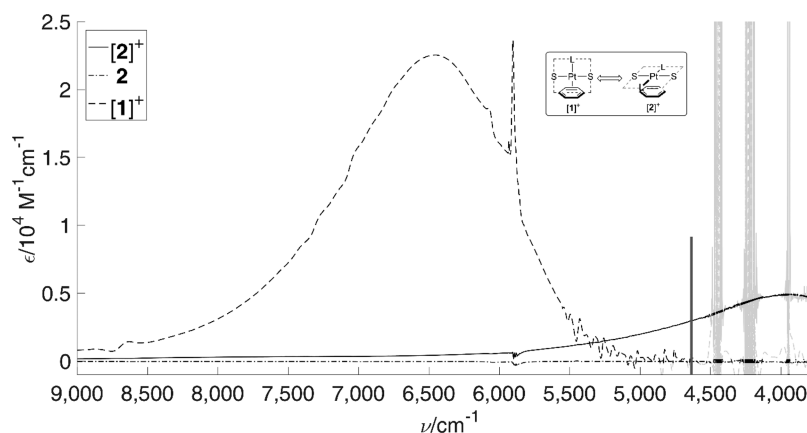
Figure 4. NIR absorption profiles of in situ generated [2]NTf$_2$, **2** and [1]NTf$_2$ in CH$_2$Cl$_2$ at T = 203 K; ε_{solv} (CH$_2$Cl$_2$) = 8.93;[22] Solid gray bar: TD-DFT derived ν_{max}(TD-DFT) = 4562 cm^{-1} (f_{osc}(TD-DFT) = 0.19); Solvent background absorption at ν_{max} < 4500 cm^{-1} attenuated (light gray) for clarity.

seem to hold for [2]$^+$ also). In line with EPR spectroscopic and structural data of [1]$^+$, a metal mediated LLIVCT type transition in a solvent averaged Class II−III system is proposed.[2] Note that both ν_{max} and ε_{max} of [1]NTf$_2$ proved to be nearly independent of temperature, as was probed in CH$_2$Cl$_2$ solution in the range of 203−298 K (cf. Table 2 and Figure 4). Spectral changes are largely dominated by the temperature dependent change of solvent density, cf. Figure S10, SI.

Intriguingly, VT absorption spectra of [2]NTf$_2$ generated in situ in CH$_2$Cl$_2$ solution at 203 K display a clearly less intense but substantially red-shifted NIR band centered at ν_{max} = 4000 cm^{-1} (2500 nm, ε_{max} = 0.6 × 10^4 M^{-1} cm^{-1}, $\Delta\nu_{1/2}$ ∼ 1700 cm^{-1}) as shown in Figure 4. The spectral features have been reproduced in a toluene-d_8 solution (cf. Figure S11, SI) as summarized in Table 2. On the basis of theoretical data, the lowest-energy transition of [2]NTf$_2$ is attributed to a CR transition within a Class III system. Solvent background absorption is strong in the ≤4500 cm^{-1} spectral region, so the complete NIR profile of [2]$^+$ could not be recorded. For this reason, the reported band widths rely on Gaussian curve fitting, and any asymmetry in the profile cannot be accounted for.

Electronic structure and TD-DFT calculations at the BLYP-35-D3/TZVP/ZORA level of theory fully support the Class II−III and Class III classifications and predict NIR transitions at 7000 and 4600 cm^{-1} for [1]$^+$ and [2]$^+$, respectively, and which are included as gray bars in Figures 3 and 4. Note that TD-DFT derived transitions generally match experimental data very well; cf. Table S9 and Figure S18, SI. Again, we find the relative orientation of the metal coordination plane to be decisive for the chromophore properties: While the β-HOMO → β-LUMO transition in [1]$^+$ is identified as a metal mediated LLIVCT along the S−Pt−S vector (Figure 5a; a detailed MO diagram is provided in Figure S16, SI), the low-energy β-HOMO → β-LUMO transition in [2]$^+$ is best described as a P−Pt LMCT augmented by a CR contribution from the electron delocalized thiophenoxyl/thiophenolato structure (Figure 5b; detailed MO diagram provided in Figure S17, SI).

The observation of a substantial decrease of ε_{max}([2]$^+$) as compared to ε_{max}([1]$^+$) is unexpected, both with respect to established models of CT band position and intensity of mixed-valent systems[2] and the outcomes of our TD-DFT studies. Despite that TD-DFT data indicate a change of the electronic character of the transition from LLIVCT in case of [1]$^+$ to a combined MLCT/CR for [2]$^+$, predicted transition probabilities are conserved, and computed oscillator strengths f_{osc} do
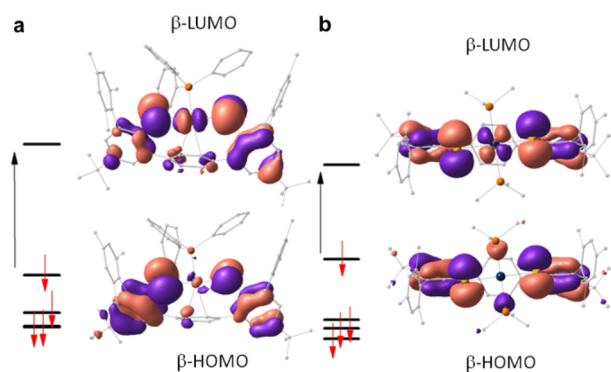
Figure 5. Kohn−Sham MOs and energy diagrams for $[1]^+$ (a) and $[2]^+$ (b) from a spin-unrestricted ZORA-BLYP-35 DFT calculations. TD-DFT derived lowest-energy transitions (β-HOMO → β-LUMO): ν_{max}(TD-DFT) = 7007 cm^{-1} for $[1]^+$ and 4562 cm^{-1} for $[2]^+$.

not differ significantly for $[1]^+$ and $[2]^+$. Since the stoichiometry of the redox chemistry of the couple $2/[2]^+$ has been proven correct (vide supra), the small values of $\varepsilon_{max}([2]^+)$ cannot be attributed to trivial concentration effects; rather the diminished value of ε_{max} is a property inherent to $[2]^+$.

Comparison with literature data does not provide a congruent picture at present. For instance, in the case of the well-studied complexes of mixed-valence salen ligands, spectral positions of the NIR bands become increasingly blue-shifted and gain intensity along the series Pd < Ni < Pt. This trend has been rationalized in terms of an enhancement of electronic coupling in the same direction.[15b] In clear contrast, the intensities (f_{osc} and ε_{max}) of the NIR bands of mixed-valence bis-benzene-1,2-dithiolato d^8-metalate complexes systematically and substantially *decrease* with increasing coupling strength, clearly opposing the trend observed for their spectral positions, ν_{max}.[6b] Obviously, the substitution of oxygen donors for sulfur results in a significant change of electronic structures, pointing to a lack of generality of the current knowledge and the scope of the conclusions made.[23]

CONCLUSIONS

The design of (electro-switchable) mixed-valent structures that allow the strength of electron coupling to be varied in a systematic fashion is a vibrant field of research. In this context, delineation of characteristic structural parameters that control electronic delocalization and associated optical properties is of pivotal importance. As a novel approach, control of the relative orientation of ligand and metal orbitals of an open-shell complex has been shown to result in spectroscopically distinct electronic structures, presenting a novel approach toward the design of NIR chromophores. The concept relies on the use of a *trans*-coordinating, redox noninnocent dithiophenol ligand of variable denticity. In general, complexes of metal-coupled mixed-valent thiyl/thiolato ligands display optical properties that are similar to, for instance, those of the well-studied family of salen-derived mixed-valent coordination compounds. On the other hand, substituting oxygen for sulfur does result in electronic structures whose properties clearly oppose general trends, and which mandates further studies to understand their electronic origin. As one approach, studies on structures with metals other than precious platinum are currently underway.

EXPERIMENTAL SECTION

All manipulations of air and moisture sensitive compounds were carried out under a dry argon atmosphere using standard Schlenk or glovebox techniques (MBraun, MB 150-GI). 1,4-terphenyldithiophenol[24] and *trans*-Pt(py)$_2$Cl$_2$[18] were prepared following literature procedures. AgClO$_4$, high purity ferrocene (Fc) were obtained from Alfa Aesar, and Fc was sublimed once prior to use. 1,1′-Diacetylferrocene (Fc″) was used as received from TCI. Benzoquinone was recrystallized 3 times from ethanol, sublimed twice (r.t., 10^{-3} mbar, static vacuum), and stored under argon. Bis(trifluoromethanesulfonyl)amine (HNTf$_2$, 99%, Acros Organics) was sublimed once before use. Solvents were purified and dried prior to use. 1,1,2,2-C$_2$H$_2$Cl$_4$ was dried over and distilled from P$_2$O$_5$, degassed, and saturated with Ar. Hexane was dried over Grubbs columns of an MBraun solvent purification system (SPS). Diethyl ether, pentane, and toluene were predried over activated 3 Å molecular sieves and distilled from sodium benzophenone ketyl under argon. Methanol was dried by percolation through a column of activated neutral alumina. Stabilizer free dichloromethane (Fisher Scientific) was first distilled from P$_2$O$_5$, then from K$_2$CO$_3$, and finally stored over activated basic alumina. Acetonitrile (MeCN) for use in electrochemical experiments was sequentially dried over and distilled from CaH$_2$ and P$_2$O$_5$, and finally percolated through activated neutral alumina. 1,2-Difluorobenzene (1,2-C$_6$F$_2$H$_4$; obtained from ABCR) was dried and purified by percolation through a column of activated neutral alumina, and distilled onto activated neutral alumina prior to use. C$_6$D$_6$ was dried over and distilled from NaK alloy whereas C$_7$D$_8$, CDCl$_3$ and CD$_2$Cl$_2$ were dried over and vacuum transferred from 3 Å molecular sieves. In general, solvents were stored over 3 Å molecular sieves under argon. Molecular sieves and alumina were activated by heating under dynamic vacuum (10^{-3} mbar) at 523 K for 24−48 h.

NMR data were recorded on a Bruker Avance II 400 and an AVII +500 spectrometer (VT NMR studies). δ values are given in ppm, J values in Hz. ^{1}H and ^{13}C{^{1}H}-NMR chemical shifts are referenced to the residual proton and naturally abundant carbon resonances of the solvents: 7.16/128.06 (C$_6$H$_6$-d_6), 5.32/53.84 (CH$_2$Cl$_2$-d_2), and 7.26/77.16 (CHCl$_3$-d) ppm. ^{31}P NMR chemical shifts are referenced to an external standard sample of 85% H$_3$PO$_4$ set to 0 ppm.

EPR spectra were collected using 4 mm O.D. Wilmad quartz (CFQ) EPR tubes on a continuous wave X-band Bruker ESP 300E spectrometer, and are referenced to the Bruker Strong Pitch standard g_{iso} = 2.0028. EPR simulations were done with EasySpin (version 5.0.21)[25] and MATLAB and Statistic Toolbox Release R2016a (The MathWOrks, Inc., Natick, Massachusetts, United States). Fitting of EPR spectra was carried out with the easyfit tool included in EasySpin package, using either pepper for solid state or garlic for solution EPR data.

Electronic spectra were recorded on PerkinElmer Lambda 1050 UV/vis/NIR and Lambda 35 UV/vis spectrometer. For VT experiments, a CoolSpeK UV USP-203-B cryostat from UNISOKU and a four-side transparent cell with screw cap and septum were used. In general, sample concentrations were corrected for temperature dependent changes of solvent density δ by using a modified form of the Rackett equation,[26] and δ(C$_7$D$_8$, 213 K) was estimated from δ(C$_7$D$_8$, 298 K) × δ(C$_7$H$_8$, 213 K)/δ(C$_7$H$_8$, 298 K), assuming $\delta(T)$ of C$_7$D$_8$ and C$_7$H$_8$ be equal in the temperature range studied.

Evan's method[27] was employed to determine μ_{eff} in solution using a coaxial insert for 5 mm NMR sample tubes, χ_M^{dia} = −0.5 × M, M = dimensionless molecular weight of the sample, χ_M^{dia}(CH$_2$Cl$_2$) = −4.66 × 10^{-5} cm^3 mol^{-1} and χ_M^{dia}(THF) = −5.3 × 10^{-5} cm^3 mol^{-1} were used to correct for diamagnetic susceptibilities of sample and solvent.[28]

X-ray diffraction data were collected on a Bruker Smart APEXII diffractometer with graphite-monochromated MoK$_\alpha$ radiation. The programs used were Bruker's APEX2 v2011.8−0, including SADABS for absorption correction and SAINT for structure solution, the WinGX suite of programs version 2013.3,[29] SHELXS and SHELXL for structure solution and refinement,[30] PLATON,[31] and Ortep.[32] Crystals were, unless otherwise noted, coated in a perfluorinated polyether oil and mounted on a 100 μm MiTeGen MicroMounts loop

that was placed on the goniometer head under a stream of dry nitrogen at 100 K.

Cyclic voltammetry (CV) measurements were performed at 290 K under argon atmosphere with a BASi CV-50W in a gastight, full-glass, three-electrode cell setup. nBu_4NPF_6 electrolyte (Alfa Aesar) was recrystallized 3 times from acetone/water and employed as a 0.1 M solution in CH_2Cl_2 and MeCN. A Pt disc electrode (Deutsche Metrohm GmbH & Co. KG, electro-active area = 0.080 ± 0.003 cm^2) and a 1 mm coiled Pt-wire were employed as working and counter electrodes. The Ag/Ag$^+$ redox couple, in the form of a 0.5 mm Ag wire in a 0.01 M AgClO$_4$/0.1 M nBu_4NPF_6 MeCN solution, served as a reference electrode. Voltammograms were corrected for capacitive currents of electrolyte solutions and overall cell resistance, and potentials are reported relative to Fc/[Fc]$^+$ in CH_2Cl_2, with $E_{1/2}$(Fc/[Fc]$^+$/0.1 M nBu_4NPF_6/CH_2Cl_2, 290 K) = 0.212 ± 0.001 V. The electro-active area of the Pt disc electrode was calculated from Fc/[Fc]$^+$ measurements in 0.1 M nBu_4NPF_6 solution in CH_2Cl_2 at various concentrations and potential sweep rates at 295 K, using D(Fc/CH_2Cl_2, 295 K) = 2.2×10^{-5} cm^2 s^{-1}.[33] The working electrode was rinsed with acetone, polished very gently with a paste of 0.3 μm alumina (Deutsche Metrohm GmbH & Co. KG) in deionized water, rinsed thoroughly with plenty of deionized water, and finally acetone after each use. Periodic Fc/[Fc]$^+$ reference measurements verified the electro-active surface area of the Pt electrode, and the stability of the potential of the Ag/Ag$^+$ reference electrode.

Numeration scheme used for 1,4-terphenyldithiophenolato ligand in coordination compounds.

= [Mes$_2^t$Bu$_2$S$_2$]$^{2-}$
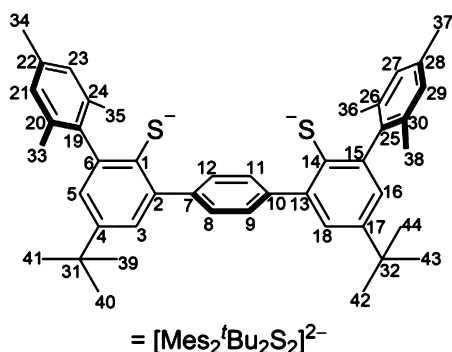
Preparation of 1,1′-Diacetylferrocenium Bis(trifluoromethylsulfonyl)imide [Fc″]NTf$_2$. To a solution of 4-benzoquinone (62 mg, 0.576 mmol) in 8 mL Et$_2$O was added dropwise a solution of HNTf$_2$ (340 mg, 1.296 mmol) in 8 mL Et$_2$O at r.t., followed by a solution of Fc″ (259 mg, 0.96 mmol) in 0.5 mL CH_2Cl_2. Within 10 min a blue-green crystalline solid separated from the stirred solution, was filtered off, washed with Et$_2$O until the washings were colorless, and finally dried under dynamic vacuum overnight at r.t. Yield: 441 mg (0.8 mmol, 78%).

UV/vis (1,1,2,2-C$_2$H$_2$Cl$_4$, 293 K): λ (ε/M^{-1} cm^{-1}) = 650 (420), 483 (252) nm. Elemental analysis calcd. (%) for C$_{16}$H$_{14}$F$_6$FeNO$_6$S$_2$: C, 34.93; H, 2.56; N, 2.55; S, 11.65; found: C, 35.29; H, 2.56; N, 2.71; S, 11.71; μ_{eff} (THF/1,1,2,2-C$_2$H$_2$Cl$_4$, 274−283 K) = 2.7(1).

Details on the molecular structure of [Fc″]NTf$_2$ are collected in Figure S12 and Table S7, SI.

Preparation of 1. Ligand Mes$_2^t$Bu$_2$(SH)$_2$ (530 mg, 0.83 mmol) and benzyl potassium (215 mg, 1.65 mmol) were reacted in 36 g of toluene at r.t. to afford a clear yellow solution, to which PPh$_3$ (216 mg, 0.83 mmol) and *trans*-Pt(py)$_2$Cl$_2$ (350 mg, 0.83 mmol) were added and stirring was continued overnight. The dark green solution was filtered from KCl, the solvent removed under vacuum, and the dark green residual solid washed with pentane, redissolved in toluene, and finally crystallized by slow diffusion of pentane vapor at r.t. to yield dark green needles of 1 × 0.5C$_7$H$_8$. Yield 462 mg (0.4 mmol, 49%).

^{1}H NMR (500 MHz, CD$_2$Cl$_2$, 298 K): δ = 7.623 (d, ^3J(H,P) = 2 Hz, ^2J(H,Pt) = 15 Hz, 4H, H-8,9,11,12), 7.32 (d, ^4J(H−H) = 2.3 Hz, 2H, H-3,18), 7.26 (m, 6H, PPh$_3$-H$_{ortho}$, ^2J(C,P) = 10 Hz), 7.23 (m, 3H, PPh$_3$-H$_{para}$, ^4J(C,P) = 3 Hz), 7.09 (m, 6H, PPh$_3$-H$_{meta}$, ^3J(C,P) =

12 Hz), 6.79 (d, ^4J(H,H) = 2.3 Hz, 2H, H-5,16), 6.60 (m, 4H, H-21,23,27,29), 2.28 (s, 6H, H-34,37), 1.709 (s, 12H, H-33,35,36,38), 1.309 (s, 18H, H-39−44) ppm. ^{13}C{^{1}H}-NMR (126 MHz, CD$_2$Cl$_2$, 298 K): δ = 145.91 (C-4,17), 140.74 (C-6,15), 140.32 (d, J(C,P) = ~1 Hz, C-7,10), 139.72 (C-19,25), 138.04 (C-2,13), 136.61 (d, ^2J(C,Pt) = 6 Hz, C-1,14), 135.93 (C-20,24,26,30), 135.34 (d, ^2J(C,P) = 10 Hz, PPh$_3$-C$_{ortho}$), 135.3 (C-22,28), 130.74 (d, ^4J(C,P) = 3 Hz, PPh$_3$-C$_{para}$), 127.73 (C-21,23,27,29), 127.68 (C-5,16), 127.44 (d, ^3J(C,P) = 12 Hz, PPh$_3$-C$_{meta}$), 126.44 (d, ^1J(C,P) = 69 Hz, PPh$_3$-C$_{ipso}$), 122.17 (C-3,18), 114.7 (broad, $\nu_{1/2}$ ~53 Hz, C-8,9,11,12), 34.42 (C-31,32), 31.51 (C-39−44), 21.15 (C-34,37), 20.35 (C-33,35,36,38) ppm. ^{31}P{^{1}H}-NMR (202 MHz, CD$_2$Cl$_2$, 298 K): δ = 33.9 (^1J(P−Pt) = 4770 Hz) ppm. ^{1}H−^{195}Pt-HSQC-NMR (500 MHz, CDCl$_3$, 298 K): δ_{Pt} = −4811 ppm. UV/vis (1,2-C$_6$F$_2$H$_4$, 293 K): λ (ε/M^{-1} cm^{-1}) = 329 (22000), 360 (16000), 430 (1100), 578 (200) nm. Elemental analysis calcd. (%) for C$_{62}$H$_{63}$PPtS$_2$: C, 68.74; H, 5.90; S, 5.60; found: C, 68.40; H, 5.58; S, 5.36.

Preparation of [1]NTf$_2$. Complex 1 (100 mg, 0.087 mmol) was dissolved in 6 mL of CH_2Cl_2 to which a solution of [FcAc$_2$]NTf$_2$ (50 mg, 0.091 mmol) in 2 mL CH_2Cl_2 was added dropwise at r.t. The resulting dark red solution was cannula-transferred into 100 mL of vigorously stirred pentane. Dark maroon needles separated at 245 K. The mother liquor was decanted and the crystals washed with pentane. Yield: 93 mg (0.067 mmol, 77%).

UV/vis/NIR (293 K): (a) C$_7$H$_8$, λ (ε/M^{-1} cm^{-1}) = 348 (13700), 374 (14000), 483 (2300), 514 (2400), 612 (1000), 762 (400), 1003 (600), 1523 (15400) nm; (b) CH_2Cl_2, 277 (50000), 351 (17700), 381 (20200), 502 (3600), 621 (1500), 775 (700), 1000 (800), 1547 (22000) nm; (c) 1,2-C$_6$F$_2$H$_4$, 352 (14000), 378 (15500), 500 (3000), 610 (1200), 767 (500), 1002 (600), 1540 (17000) nm; (d) C$_4$H$_6$O$_3$, 270 (41300), 349 (15300), 377 (16000), 521 (2700), 615 (1200), 776 (500), 1520 (16200) nm. μ_{eff} = 2.3 (213−313 K, CD$_2$Cl$_2$ containing 1,1,2,2-C$_2$H$_4$Cl$_4$). Elemental analysis calcd. (%) for C$_{64}$H$_{63}$F$_6$NO$_4$PPtS$_4$: C, 55.76; H, 4.61; N, 1.02; S, 9.30; found: C, 53.97; H, 4.09; N, 1.17; S, 8.88. Elemental analysis of different batches of [1]NTf$_2$ have consistently yielded lower than expected values for C, H, and S. Especially, determination of H and S composition is biased in some of the samples due to difficulties desorbing H$_2$O and SO$_2$ properly separated from the device column. For this reason, the chemical identity of [1]NTf$_2$ has been analyzed by high resolution ESI-MS from a THF solution of the compound.[M]$^+$ calculated: 1097.37512; found: 1097.37753, deviation: 1.75 ppm; cf. to Figure S1, SI, for details.

Preparation of 2. To a suspension of 1 (100 mg, 0.087 mmol) in 4 mL of hexane were added 0.95 mL 0.2 M PMe$_3$ in toluene at r.t. A clear yellow solution formed, from which the solvent was removed under vacuum. Crystallization from C$_6$H$_6$/methanol afforded yellow needles of 2 × 2MeOH. Yield 67 mg (0.06 mmol, 73%). Methanol is removed by coevaporation of a C$_6$H$_6$ solution of 2 × 2MeOH. For this reason, samples of 2 usually contain ~0.17 equiv of residual C$_6$H$_6$.

^{1}H NMR (400 MHz, CDCl$_3$, 298 K): δ = 7.38 (s, 4H, H-8,9,11,12), 7.347 (d, ^4J(H,H) = 2.5 Hz, 2H, H-3,18), 6.909 (m, 4H, H-21,23,27,29), 6.855 (d, ^4J(H,H) = 2.5 Hz, 2H, H-5,16), 2.32 (s, 6H, H-34,37), 2.069 (s, 12H, H-33,35,36,38), 1.325 (s, 18H, H-39−44), 1.268 (N-line pattern, $^{|2+4|}J$(H,P) = 7 Hz, 18H, ^3J(H,Pt) = 25 Hz, *trans*-PMe$_3$) ppm. ^{13}C{^{1}H} NMR (101 MHz, CDCl$_3$, 298 K): δ = 143.79 (C-4,17), 141.69 (C-6,15), 141.09 (C-19,25), 140.26 (C-7,10), 140.09 (C-2,13), 137.14 (C-1,14), 136.22 (C-20,24,26,30), 135.46 (C-22,28), 127.85 (C-21,23,27,29), 127.8 (C-8,9,11,12), 126.31 (C-5,16), 123.91 (C-3,18), 34.06 (C-31,32), 31.46 (C-39−44), 21.29 (C-34,37), 20.49 (C-33,35,36,38), 12.64 (N-line pattern, $^{|1+3|}J$(C,P) = 37 Hz, *trans*-PMe$_3$) ppm. ^{31}P{^{1}H} NMR (162 MHz, CDCl$_3$, 298 K): δ = −20.9 (^1J(P,Pt) = 2870 Hz) ppm. ^{1}H−^{195}Pt-HSQC-NMR (500 MHz, CDCl$_3$, 298 K): δ_{Pt} = −4220 ppm. UV/vis/NIR (1,2-C$_6$F$_2$H$_4$, 293 K): λ (ε/M^{-1} cm^{-1}) = 318 (14000) nm. Elemental analysis calcd. (%) for C$_{50}$H$_{66}$P$_2$PtS$_2$: C, 60.77; H, 6.73; S, 6.49; found: C, 60.12; H, 6.30; S, 6.14.

UV/Vis/NIR Measurements. One mM stock solutions of 1, [1]NTf$_2$, and 2 in 1,2-C$_6$F$_2$H$_4$ and of [Fc″]NTf$_2$ in 1,1,2,2-tetrachloroethane were prepared and spectra with concentrations

between 0.2 mM and 5 μM were recorded to determine exctinction coefficients.

UV/vis/NIR electronic absorption data of [**2**]NTf$_2$ were collected from an in situ prepared sample. Stock solutions of **2** (1.7 mM), [Fc″]NTf$_2$ (2.4 mM), and Fc″ (0.8 mM) were prepared in CH$_2$Cl$_2$ and reference spectra were obtained at different temperatures. 2.8 mL CH$_2$Cl$_2$ was filled in a four-side transparent cell with screw cap and septum. After cooling to 203 K, 0.195 mL stock solution of **2** (0.33 μmol) were added. Under stirring 0.25 equiv of [Fc″]NTf$_2$ were added and a spectrum was recorded. This procedure was repeated three times. Spectra of CH$_2$Cl$_2$ were collected at the same temperature and subtracted for background correction.

UV/vis/NIR of [**2**]NTf$_2$ (203 K): (a) CH$_2$Cl$_2$, λ (ε/M^{-1} cm^{-1}) = 510 (2600), 632 (2000), 870 (500), 1340 (400), 2500 (6000) nm; (b) C$_7$D$_8$, 513 (2700), 640 (1900), 866 (600), 2470 (4000) nm.

Computational Details. All DFT calculations were performed using ORCA2.9.1.[34] TZVP basis sets[35] were used throughout. The presence of platinum was accounted for with van Wüllen's zero order regular approximation (ZORA),[36] implying TZV-ZORA auxiliary basis sets.[36b] Geometric structure optimizations were performed with the GGA functional BP86[37] starting from the experimental atom positions of **1**, [**1**]NTf$_2$, and **2**. Dispersion contributions were approximated using Grimme's DFT-D3 atom-pairwise dispersion corrections.[38] Numerical frequency calculations for [**2**]$^+$ gave no imaginary modes and revealed the optimized structures to be a stationary point on the energy surface. It is noted that the frequency calculation of [**1**]$^+$ gave one low-frequency imaginary mode due to methyl-group rotation. Computed Mulliken spin densities are tabulated in Table S8, SI. UV/vis/NIR spectroscopic properties were extracted from single-point TD-DFT calculations (BP86, B3LYP[39] and BLYP-35[20]) in the BP86-optimized atomic positions. The computational methodology was validated by respective calculations on the platinate(II) complex [Pt(tdt)$_2$]$^-$, tdt = 4-Me-1,2-benzenedithiophenol, reported by Gray et al.,[6a] and was found to reproduce the original experimental data (cf. Figure S15, SI). The MO diagram fully reproduces the previous DFT analysis of the *tert*-butyl substituted congener by Neese and Wieghardt et al.[6b]

ASSOCIATED CONTENT

Ⓢ Supporting Information

The Supporting Information is available free of charge on the ACS Publications website at DOI: 10.1021/jacs.6b13085.

Experimental procedures, spectra, crystallographic details, calculated structures, and TD-DFT data (PDF)
Crystal data (CIF)
Crystal data (CIF)

AUTHOR INFORMATION

Corresponding Authors
*andreas.berkefeld@anorg.uni-tuebingen.de
*gerald.hoerner@tu-berlin.de

ORCID ⓘ
Andreas Berkefeld: 0000-0002-2757-7841

Notes
The authors declare no competing financial interest.

ACKNOWLEDGMENTS

REFERENCES

(1) (a) Kaim, W. *Coord. Chem. Rev.* **2011**, *255*, 2503−2513. (b) Mortimer, R. J. *Annu. Rev. Mater. Res.* **2011**, *41*, 28. (c) Ward, M. D. *J. Solid State Electrochem.* **2005**, *9*, 778−787.

(2) (a) Demadis, K. D.; Hartshorn, C. M.; Meyer, T. J. *Chem. Rev.* **2001**, *101*, 2655−2686. (b) D'Alessandro, D. M.; Keene, F. R. *Chem. Rev.* **2006**, *106*, 2270−2298.

(3) König, E.; Kremer, S. *Chem. Phys. Lett.* **1970**, *5*, 87−90.

(4) Tang, J.-H.; Yao, C.-J.; Cui, B.-B.; Zhong, Y.-W. *Chem. Rec.* **2016**, *16*, 754−767.

(5) Deibel, N.; Schweinfurth, D.; Fiedler, J.; Zalis, S.; Sarkar, B. *Dalton Trans.* **2011**, *40*, 9925−9934.

(6) (a) Williams, R.; Billig, E.; Waters, J. H.; Gray, H. B. *J. Am. Chem. Soc.* **1966**, *88*, 43−50. (b) Ray, K.; Weyhermüller, T.; Neese, F.; Wieghardt, K. *Inorg. Chem.* **2005**, *44*, 5345−5360. (c) Ray, K.; Petrenko, T.; Wieghardt, K.; Neese, F. *Dalton Trans.* **2007**, 1552−1566. (d) Maiti, B. K.; Maia, L. B.; Pal, K.; Pakhira, B.; Avilés, T.; Moura, I.; Pauleta, S. R.; Nuñez, J. L.; Rizzi, A. C.; Brondino, C. D.; Sarkar, S.; Moura, J. J. G. *Inorg. Chem.* **2014**, *53*, 12799−12808. (e) Machata, P.; Herich, P.; Lušpai, K.; Bucinsky, L.; Šoralová, S.; Breza, M.; Kozisek, J.; Rapta, P. *Organometallics* **2014**, *33*, 4846−4859.

(7) Arumugam, K.; Shaw, M. C.; Chandrasekaran, P.; Villagrán, D.; Gray, T. G.; Mague, J. T.; Donahue, J. P. *Inorg. Chem.* **2009**, *48*, 10591−10607.

(8) (a) Kramer, W. W.; Cameron, L. A.; Zarkesh, R. A.; Ziller, J. W.; Heyduk, A. F. *Inorg. Chem.* **2014**, *53*, 8825−8837. (b) Zanello, P.; Corsini, M. *Coord. Chem. Rev.* **2006**, *250*, 2000−2022. (c) Pierpont, C. G. *Coord. Chem. Rev.* **2001**, *216−217*, 99−125. (d) Haga, M.; Dodsworth, E. S.; Lever, A. B. P. *Inorg. Chem.* **1986**, *25*, 447−453.

(9) Sarkar, B.; Schweinfurth, D.; Deibel, N.; Weisser, F. *Coord. Chem. Rev.* **2015**, *293−294*, 250−262.

(10) (a) Eisenberg, R.; Gray, H. B. *Inorg. Chem.* **2011**, *50*, 9741−9751. (b) Garreau-de Bonneval, B.; Moineau-Chane Ching, K. I.; Alary, F.; Bui, T.-T.; Valade, L. *Coord. Chem. Rev.* **2010**, *254*, 1457−1467. (c) Aragoni, M. C.; Arca, M.; Cassano, T.; Denotti, C.; Devillanova; Francesco, A.; Frau, R.; Isaia, F.; Lelj, F.; Lippolis, V.; Nitti, L.; Romaniello, P.; Tommasi, R.; Verani, G. *Eur. J. Inorg. Chem.* **2003**, *2003*, 1939−1947.

(11) (a) Leung, W.-H.; Chan, E. Y. Y.; Chow, E. K. F.; Williams, I. D.; Peng, S.-M. *J. Chem. Soc., Dalton Trans.* **1996**, 1229−1236. (b) Pratt, R. C.; Stack, T. D. P. *J. Am. Chem. Soc.* **2003**, *125*, 8716−8717. (c) Shimazaki, Y.; Tani, F.; Fukui, K.; Naruta, Y.; Yamauchi, O. *J. Am. Chem. Soc.* **2003**, *125*, 10512−10513. (d) Thomas, F. *Dalton Trans.* **2016**, *45*, 10866−10877. (e) Kurahashi, T.; Fujii, H. *J. Am. Chem. Soc.* **2011**, *133*, 8307−8316.

(12) Stenson, P. A.; Board, A.; Marin-Becerra, A.; Blake, A. J.; Davies, E. S.; Wilson, C.; McMaster, J.; Schröder, M. *Chem. - Eur. J.* **2008**, *14*, 2564−2576.

(13) (a) Shimazaki, Y.; Yajima, T.; Tani, F.; Karasawa, S.; Fukui, K.; Naruta, Y.; Yamauchi, O. *J. Am. Chem. Soc.* **2007**, *129*, 2559−2568. (b) Storr, T.; Verma, P.; Pratt, R. C.; Wasinger, E. C.; Shimazaki, Y.; Stack, T. D. P. *J. Am. Chem. Soc.* **2008**, *130*, 15448−15459.

(14) Orio, M.; Jarjayes, O.; Kanso, H.; Philouze, C.; Neese, F.; Thomas, F. *Angew. Chem., Int. Ed.* **2010**, *49*, 4989−4992.

(15) (a) Storr, T.; Wasinger, E. C.; Pratt, R. C.; Stack, T. D. P. *Angew. Chem., Int. Ed.* **2007**, *46*, 5198−5201. (b) Shimazaki, Y.; Stack, T. D. P.; Storr, T. *Inorg. Chem.* **2009**, *48*, 8383−8392.

(16) (a) Rotthaus, O.; Jarjayes, O.; Perez Del Valle, C.; Philouze, C.; Thomas, F. *Chem. Commun.* **2007**, 4462−4464. (b) Kochem, A; Orio, M.; Jarjayes, O.; Neese, F.; Thomas, F. *Chem. Commun.* **2010**, *46*, 6765−6767. (c) Chiang, L.; Kochem, A; Jarjayes, O.; Dunn, T. J.; Vezin, H.; Sakaguchi, M.; Ogura, T.; Orio, M.; Shimazaki, Y.; Thomas, F.; Storr, T. *Chem. - Eur. J.* **2012**, *18*, 14117−14127.

(17) Rotthaus, O.; Thomas, F.; Jarjayes, O.; Philouze, C.; Saint-Aman, E.; Pierre, J.-L. *Chem. - Eur. J.* **2006**, *12*, 6953−6962.

(18) Kauffman, G. B.; Cowan, D. O.; Slusarczuk, G.; Kirschner, S., In *Inorg. Synth.*; Kleinberg, J., Ed.; John Wiley & Sons, Inc.: Hoboken, NJ, 1963; Vol. 7, pp 239−245.

(19) CCDC 1511080−1511083 contain the crystallographic data for this paper. These data are provided free of charge by The Cambridge Crystallographic Data Centre. See Tables S6−S7, SI, for details.

(20) Parthey, M.; Kaupp, M. *Chem. Soc. Rev.* **2014**, *43*, 5067−5088.

(21) Loughrey, J. J.; Sproules, S.; McInnes, E. J. L.; Hardie, M. J.; Halcrow, M. A. *Chem. - Eur. J.* **2014**, *20*, 6272−6276.

(22) Speight, J. G.; Lange, N. A. *Lange's Handbook of Chemistry*, 16th ed.; McGraw-Hill: New York, 2004.

(23) Solomon, E. I.; Xie, X.; Dey, A. *Chem. Soc. Rev.* **2008**, *37*, 623−638.

(24) Koch, F.; Schubert, H.; Sirsch, P.; Berkefeld, A. *Dalton Trans.* **2015**, *44*, 13315−13324.

(25) Stoll, S.; Schweiger, A. *J. Magn. Reson.* **2006**, *178*, 42−55.

(26) Yaws, C. L. *Chemical Properties Handbook: Physical, Thermodynamic, Environmental, Transport, Safety, and Health Related Properties for Organic and Inorganic Chemicals*; McGraw-Hill: New York, 1999; pp VII, 779.

(27) Evans, D. F. *J. Chem. Soc.* **1959**, 2003−2005.

(28) Bain, G. A.; Berry, J. F. *J. Chem. Educ.* **2008**, *85*, 532.

(29) Farrugia, L. *J. Appl. Crystallogr.* **1999**, *32*, 837−838.

(30) (a) Hubschle, C. B.; Sheldrick, G. M.; Dittrich, B. *J. Appl. Crystallogr.* **2011**, *44*, 1281−1284. (b) Sheldrick, G. *Acta Crystallogr., Sect. A: Found. Crystallogr.* **2008**, *64*, 112−122.

(31) Spek, A. *Acta Crystallogr., Sect. D: Biol. Crystallogr.* **2009**, *65*, 148−155.

(32) Farrugia, L. *J. Appl. Crystallogr.* **2012**, *45*, 849−854.

(33) Janisch, J.; Ruff, A.; Speiser, B.; Wolff, C.; Zigelli, J.; Benthin, S.; Feldmann, V.; Mayer, H. A. *J. Solid State Electrochem.* **2011**, *15*, 2083−2094.

(34) Neese, F. *WIREs Comput. Mol. Sci.* **2012**, *2*, 73−78.

(35) Schäfer, A.; Horn, H.; Ahlrichs, R. *J. Chem. Phys.* **1992**, *97*, 2571−2577.

(36) (a) van Wüllen, C. *J. Chem. Phys.* **1998**, *109*, 392−399. (b) Pantazis, D. A.; Chen, X.-Y.; Landis, C. R.; Neese, F. *J. Chem. Theory Comput.* **2008**, *4*, 908−919.

(37) Becke, A. D. *Phys. Rev. A: At., Mol., Opt. Phys.* **1988**, *38*, 3098−3100.

(38) (a) Grimme, S. *J. Comput. Chem.* **2006**, *27*, 1787−1799. (b) Grimme, S.; Ehrlich, S.; Goerigk, L. *J. Comput. Chem.* **2011**, *32*, 1456−1465.

(39) (a) Becke, A. D. *J. Chem. Phys.* **1993**, *98*, 5648−5652. (b) Lee, C.; Yang, W.; Parr, R. G. *Phys. Rev. B: Condens. Matter Mater. Phys.* **1988**, *37*, 785−789.